JOURNAL OF CATALYSIS 144, 361–376 (1993)

# The Effect of Hydrogen Coadsorption on the Thermal Chemistry of Methyl Iodide on Ni(100) Surfaces

SARIWAN TJANDRA AND FRANCISCO ZAERA[1]

*Department of Chemistry, University of California at Riverside, Riverside, California 92521*

Received April 29, 1993; revised July 12, 1993

A detailed investigation of the surface chemistry of methyl iodide with preadsorbed hydrogen on Ni(100) is reported here. TPD data indicate that, in general, the presence of hydrogen on the surface induces a yield increase in methane formation and a reduction of the extent to which methyl species decompose as compared with the case where the methyl iodide is adsorbed by itself on a clean surface. Furthermore, two very different methane desorption regimes are observed at 150 and 220 K. By using both isotopically labelled methyl iodide and deuterium ($D_2$ + $CH_3I$ and $H_2$ + $CD_3I$) it was determined that while the high-temperature methane is formed via the reductive elimination of surface methyl species produced by decomposition of methyl iodide with coadsorbed hydrogen atoms, the lower temperature methane TPD peak may be the result of a direct attack of the surface hydrogen on adsorbed methyl iodide molecules in a concerted fashion instead. The TPD data also indicate that neither methylene nor methylidyne intermediates form during the decomposition of methyl iodide on nickel below 200 K, and experiments with $CH_2I_2$ clearly show that methylene species can be easily hydrogenated to methane in the presence of $D_2$ coadsorption at quite low temperatures. Finally, no H–D exchange between methyl species and coadsorbed hydrogen ($H_2$) was observed. 

## 1. INTRODUCTION

Recent studies have shown that alkyl halides, the iodides in particular, dissociate easily on metal surfaces upon thermal treatment to form adsorbed alkyl fragments and iodine atoms (*1*). Since hydrocarbon moieties like those formed by alkyl halide decomposition are believed to be important intermediates in catalytic reactions such as Fischer–Tropsch synthesis and alkane activation (*2–4*), it is hoped that the study of the surface chemistry of such species under controlled ultrahigh vacuum conditions will provide important information on the mechanism of the high pressure processes. Hydrogen preadsorption has in fact been shown to be a good method for simulating reducing catalytic reactions under vacuum (*5–9*): a few coadsorption studies using alkyl halides and hydrogen have already been reported, and their implications for catalytic systems have been somewhat assessed (*10, 11*).

As part of our ongoing studies on the chemistry of alkyl halides on metal surfaces (*1, 11–20*), in this report we present results from investigations on the reactivity of methyl iodide on Ni(100) in the presence of coadsorbed hydrogen. Previous results indicate that when adsorbed on clean Ni(100) surfaces methyl iodide dissociates to yield methyl groups and iodine atoms, and that the methyl moieties subsequently react either by incorporating a surface hydrogen atom to form methane or by dehydrogenating to surface carbon. The TPD experiments reported here show that hydrogen coadsorption inhibits the latter dehydrogenation pathway, increases the yield for methane formation, and induces the formation of some methane at temperatures significantly lower than those required in the absence of hydrogen coadsorption, presumably by opening a new pathway which involves a direct attack of a hydrogen atom on an intact adsorbed methyl iodide molecule (a bimolecular nucleophilic substitu-



0021-9517/93 $5.00

tion). The present study also indicates that neither methylene nor methylidyne intermediates form from methyl moieties on the nickel surface below 200 K, and that no H–D exchange reactions occur between methyl species and coadsorbed deuterium atoms under the conditions of our experiments.

## 2. METHODS

The ultrahigh vacuum (UHV) apparatus used in this study, decribed in detail elsewhere (*12, 17, 18*), is evacuated to a base pressure of less than $1 \times 10^{-10}$ Torr, and contains instrumentation for thermal-programmed desorption (TPD), X-ray photoelectron (XPS), static secondary ion mass (SSIMS), Auger electron (AES), and ion scattering (ISS) spectroscopies. The details of the experimental procedures used for the TPD and XPS experiments have also been reported before (*17–19*). Briefly, the TPD experiments were done using a mass quadrupole with an electron impact ionizer located inside an enclosed compartment which has two small apertures in its front and back for gas sampling and exit to the quadrupole rods respectively. The nickel crystal was positioned within 1 mm of the front aperture in order to obtain an enhancement in sensitivity for the detection of gases desorbing from the front face of the substrate and additional discrimination against desorption from the edges and back of the crystal and from the supporting wires. The mass spectrometer was interfaced to a computer in order to acquire desorption data for up to 10 different masses simultaneously in a single desorption experiments; the TPD spectra reported here were deconvolved for contributions due to other species except when otherwise indicated. A heating rate of about 10 K/s was used in the TPD runs.

XPS spectra were taken using an X-ray source with an aluminum anode and a hemispherical electron energy analyzer set to a constant pass energy that corresponded to a resolution of about 1.2 eV full width at half maximum. The absolute energy scale was calibrated against reported values for the Pt $4f_{7/2}$ and Cu $2p_{3/2}$ signals and is accurate with 0.1 eV, and the reported data were obtained after subtracting the signal obtained for the clean surface. The kinetic measurements were obtained isothermally by following the signal intensity at a binding energy of 620.4 eV as a function of time after heating the sample rapidly from 100 K to the reaction temperature, a process that was initiated after 30 s of data acquisition and that took about 2–3 s.

The nickel single crystal was cut and polished in the (100) orientation by using standard procedures, and mounted in a manipulator so it could be cooled to liquid-nitrogen temperatures and resistively heated to above 1500 K. The crystal temperature was carefully monitored with a chromel–alumel thermocouple spot-welded onto the edge of the crystal. Cleaning of the nickel surface by cycles of oxygen treatment, ion sputtering, and annealing to 1300 K were done prior to each experiment until no impurities were detected by either AES or XPS. $CH_3I$ (minimum purity of 99%) and $CD_3I$ (99.5% D) were obtained from Alfa Products and Cambridge Isotope Laboratories respectively, and were purified by following several freeze–pump–thaw cycles before dosing them into the vacuum chamber; their purity was checked periodically by mass spectrometry. Ultrahigh purity hydrogen (99.999%) and deuterium (99.5%) gases were purchased from Matheson Gas Products and used without further purification.

## 3. RESULTS

We start here by summarizing the main results obtained for methyl iodide when chemisorbed alone on Ni(100) (*18*). That data indicate that methyl iodide adsorption is molecular at low temperatures, and that the value for the sticking coefficient is about 0.05 monolayers/L and constant up to saturation, which is reached at exposures of around 4 L. Upon thermal treatment of the sample the C–I bond breaks first, a reaction that starts around 120 K, that requires about

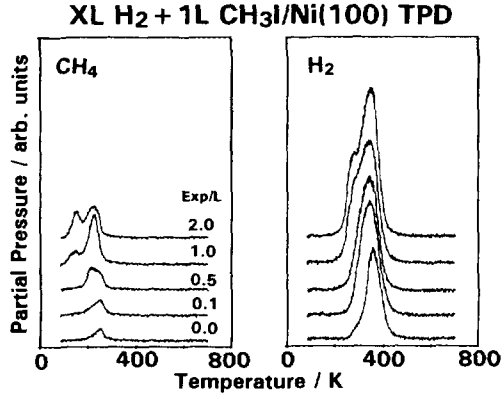


FIG. 1. Methane (a, left) and hydrogen (b, right) TPD spectra from 1 L normal methyl iodide ($CH_3I$) adsorbed on Ni(100) as a function of hydrogen preexposures. The heating rate in these experiments was about 10 K/s.

3.5 kcal/mol of energy for its activation, and that produces atomic iodine and methyl moieties on the surface. Two subsequent reactions were observed in this system at higher temperatures, namely, complete dehydrogenation to hydrogen and surface carbon (the only pathway available at low coverages), and reductive elimination with methane formation (which dominates at coverages near saturation); no coupling or polymerization reactions were ever seen in this system. Finally, even though the hydrogenation step does occur on surfaces dosed exclusively with methyl iodide, it is enhanced considerably by the presence of coadsorbed hydrogen.

In order to better understand the effect that surface hydrogen has on the chemistry of adsorbed methyl iodide, experiments were performed on surfaces where either hydrogen or deuterium was dosed before methyl iodide chemisorption. Methane and hydrogen were the only two desorbing products detected in most cases, but molecular desorption was also observed at high hydrogen coverages. Figure 1a, which shows methane TPD results obtained after the sequentially exposure of a clean Ni(100) to various amounts of hydrogen and to 1 L $CH_3I$ at 90 K, indicates that the yield for methane desorption increases with hydrogen coadsorption, and that the original methane peak, initially centered at 250 K, shifts down to 230 K. In addition, a second low temperature feature starts to grow at about 150 K after a $H_2$ predose of 1 L, and increases in intensity with increasing $H_2$ exposure while maintaining the same peak position. Using Redhead's equation (*21*) and a preexponential factor of $10^{13}\ s^{-1}$ we estimate this latter peak to correspond to an activation energy of about 9 kcal/mol, significantly lower than the 16 kcal/mol value obtained for methane formation from methyl iodide when adsorbed alone (*18*). The total yield for methane desorption increases about five times in going from $CH_3I$ dosed on a clean surface to when 2 L $H_2$ is adsorbed prior to the methyl iodide exposure.

Figure 1b shows the hydrogen thermal desorption spectra obtained for the same sequential adsorptions of $H_2$ and 1 L $CH_3I$. Hydrogen desorption starts at a peak centered around 355 K for the case of pure methyl iodide, and its total area increases with increasing predoses of hydrogen while its maximum shifts to lower temperatures. This desorption is the result of a combination of both the production of hydrogen from decomposition of $CH_3$ species on the surface and the presence of coadsorbed hydrogen; the fact that the behavior observed in this case is almost identical to that seen for hydrogen adsorbed on a clean surface suggests that the hydrogen detection in the methyl iodide case is limited by the recombination and desorption of surface hydrogen, and that methyl iodide decomposition takes place at lower temperatures. A small shoulder also develops in the low temperature side of the $H_2$ TPD spectra after hydrogen predoses above 1 L, perhaps due to some type of repulsive interaction between the different surface species (see below).

Figure 2 displays similar TPD spectra for the coadsorption of various coverages of hydrogen with a 3-L dose of methyl iodide. The main methane peak in this case is centered at

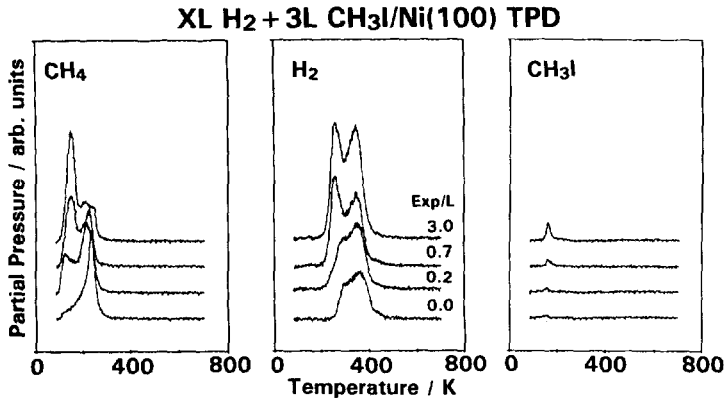


FIG. 2. Methane (a, left), hydrogen (b, center), and methyl iodide (c, right) TPD spectra from 3 L $CH_3I$ adsorbed on Ni(100) as a function of hydrogen preexposures.

240 K even in the absence of hydrogen (Fig. 2a), and the yield for the low temperature methane formation induced by hydrogen coadsorption increases to more than 70% of the total methane production. Furthermore, the low temperature shoulder (260 K) that appears in the hydrogen TPD spectra as hydrogen is coadsorbed with methyl iodide becomes a major feature (Fig. 2b). Finally, a small amount of methyl iodide molecular desorption occurs around 160 K in the presence of coadsorbed hydrogen (Fig. 2c); an activation energy of about 5.5 kcal/mol was calculated for this methyl iodide desorption by using a leading edge analysis (*22*).

Results from additional TPD experiments using deuterium and deuterated methyl iodide are shown in Figs. 3–11. Figure 3, which displays TPD spectra for the case of 3 L $D_2$ and 3 L $CH_3I$ adsorbed sequentially on Ni(100) at 90 K, shows that only $H_2$, HD, $D_2$, $CH_4$, and $CH_3D$ desorb from the surface in this system; other types of methane, namely, $CH_2D_2$, $CHD_3$, or $CD_4$, were not detected, indicating that no exchange takes place between the $CH_3$ surface species and D atoms, and likewise, no $C_2$ compounds (ethane or ethylene) were detected either, a result that rules out any possibility of carbon-carbon coupling reactions on this surface. The spectra displayed in Fig. 4 correspond to $CH_4$ and $CH_3D$ TPD data for a 1-L $CH_3I$ exposure as a function of $D_2$ predose, and show that the intensity of the 240 K $CH_4$ peak increases slightly initially as the amount of $D_2$ coadsorption increases from 0.2 to 0.5 L but then decreases at higher exposures at the expense of $CH_3D$

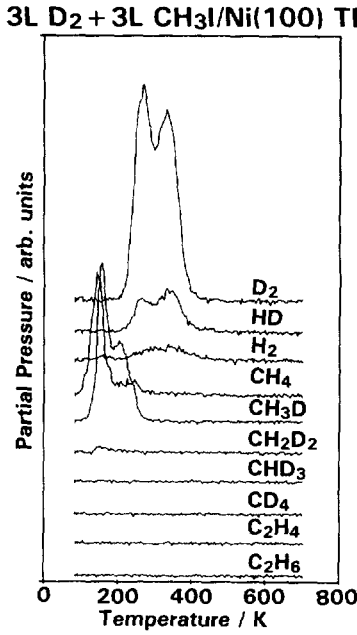


FIG. 3. TPD from a Ni(100) surface dosed sequentially with 3 L $D_2$ and 3 L $CH_3I$ at 90 K. Shown are traces for $D_2$, HD, $H_2$, $CH_4$, $CH_3D$, $CH_2D_2$, $CHD_3$, $CD_4$, $C_2H_4$, and $C_2H_6$ desorption.

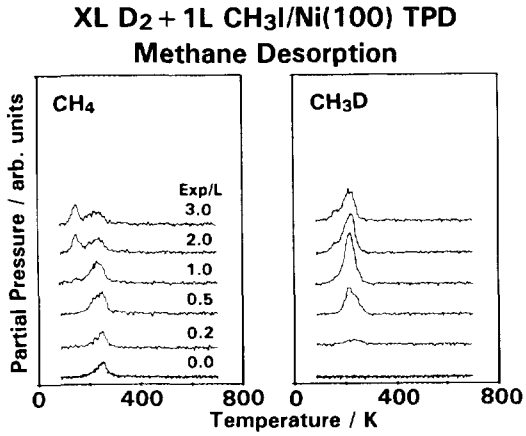


FIG. 4. $CH_4$ (a, left) and $CH_3D$ (b, right) TPD spectra from 1 L normal methyl iodide adsorbed on Ni(100) following various deuterium exposures.

formation, and that an additional low temperature methane peak appears at about 150 K in both $CH_4$ and $CH_3D$ TPD spectra (only as a small shoulder in the latter, perhaps because of a kinetic isotope effect that favors the reaction with normal hydrogen).

The desorption spectra for $H_2$, HD, and $D_2$ from various doses of $D_2$ and 1 L $CH_3I$ are shown in Fig. 5. Only $H_2$ desorption, coming both from background adsorption (about 5% of saturation) and from decomposition of methyl iodide, is seen about 350 K in the absence of $D_2$ coadsorption, but additional peaks develop around 340 K for HD and $D_2$ desorption after predosing deuterium on the surface. It should be noted that the desorption of $H_2$, HD, and $D_2$ from this $D_2$ + $CH_3I$ system all exhibit a similar behavior than that obtained from adsorption of $D_2$ alone on a clean Ni(100) surface except for the fact that in the methyl iodide coadsorption experiments an additional peak grows at about 270 K near and above saturation coverages of $D_2$. Also, while the HD yield remains relatively constant throughout the $D_2$ coverage range studied here, the $H_2$ yield decreases with increasing $D_2$ coadsorption, indicating that the extent of the methyl iodide decomposition is reduced significantly.

Similar TPD spectra were obtained from $D_2$ coadsorbed with 3 L $CH_3I$. The main difference in the hydrogen TPD results with respect to the case of the lower dose is that the low temperature peak, barely observable then, now displays significantly larger yields, especially in the case of $D_2$ desorption (Fig. 6). The fact that the deuterium yield is the one that increases the most suggests that this process is not due to the decomposition of methyl groups but to some kind of repulsive interaction between the adsorbed hydrogen (deuterium) and the iodine atoms that result from methyl iodide

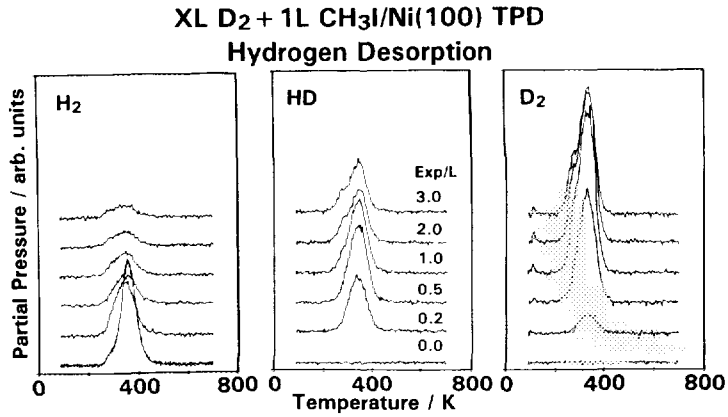


FIG. 5. $H_2$ (a, left), HD (b, center), and $D_2$ (c, right) TPD spectra from 1 L normal methyl iodide adsorbed on Ni(100) following various amounts of $D_2$.

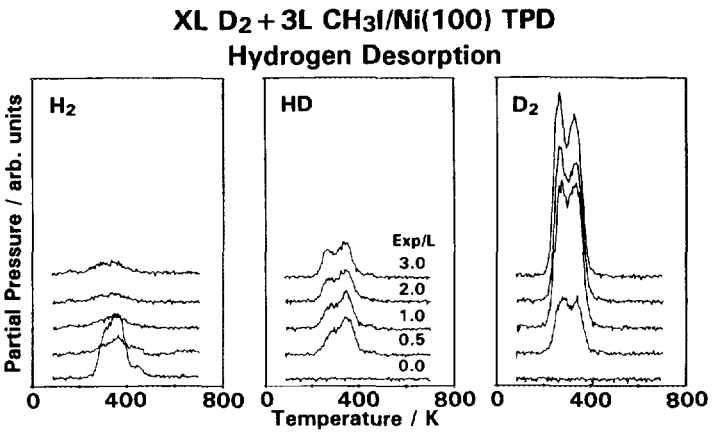


FIG. 6. $H_2$ (a, left), HD (b, center), and $D_2$ (c, right) TPD spectra from 3 L $CH_3I$ adsorbed on Ni(100) following various amounts of $D_2$.

decomposition. Also, both $CH_4$ and $CH_3D$ desorb in two regimes at about 150 and 230 K as in the low coverage case, but now the lower temperature peak dominates at high $D_2$ coadsorption coverages (Fig. 7).

The results from thermal desorption studies on the coadsorption of hydrogen ($H_2$) and fully deuterated methyl iodide ($CD_3I$) are summarized in Figs. 8–11. Figure 8 shows methane TPD spectra for various doses of hydrogen followed by a 1-L exposure of $CD_3I$: only a small amount of $CD_4$ desorbs around 260 K regardless of the amount of predosed hydrogen present on the surface (about the same in all cases), an observation that leads us to believe that this $CD_4$ may be formed at surface defects. However, $CHD_3$ desorption, which is nonexistant in the absence of coadsorbed hydrogen, develops as a single peak in the presence of 0.5 L predosed $H_2$, and splits into two peaks with larger $H_2$ doses. The TPD profiles for hydrogen desorption from the same system are shown in Fig. 9. For 1-L $CD_3I$ adsorption alone, desorption of $H_2$, HD, and $D_2$ re-

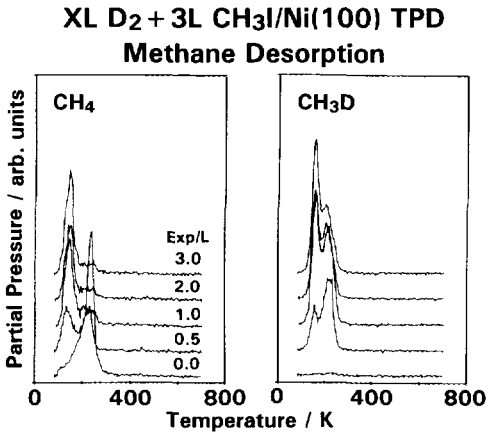


FIG. 7. $CH_4$ (a, left) and $CH_3D$ (b, right) TPD spectra from 3 L normal methyl iodide adsorbed on Ni(100) following various deuterium exposures.

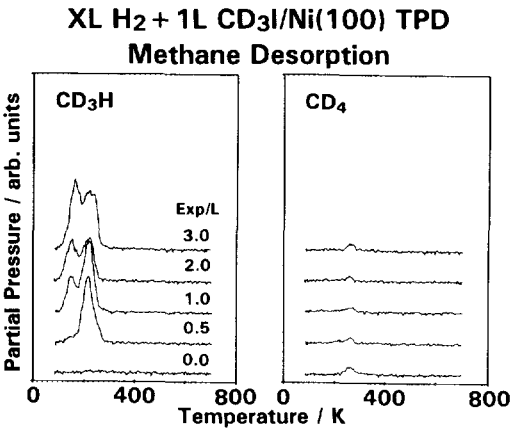


FIG. 8. $CHD_3$ (a, left) and $CD_4$ (b, right) TPD spectra from 1 L fully deuterated methyl iodide ($CD_3I$) adsorbed on a Ni(100) surface predosed with various hydrogen exposures.

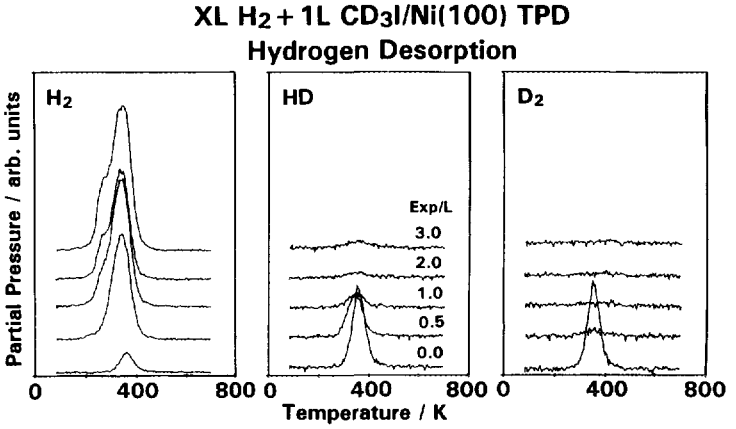


FIG. 9. $H_2$ (a, left), HD (b, center), and $D_2$ (c, right) TPD spectra from 1 L deuterated methyl iodide adsorbed on a Ni(100) surface predosed with various hydrogen exposures.

sulting from the recombination of deuterium atoms from methyl iodide decomposition with background hydrogen is seen around 360 K, but as the $H_2$ coadsorption exposure increases, the $D_2$ (and later even the HD) signal disappears: the decomposition of the $CD_3$ species is inhibited, and the hydrogenation pathway becomes dominant. The $H_2$ TPD shows the increase in $H_2$ intensity expected and the development of the low temperature shoulder at saturation seen for the other isotopic substitution cases discussed above.

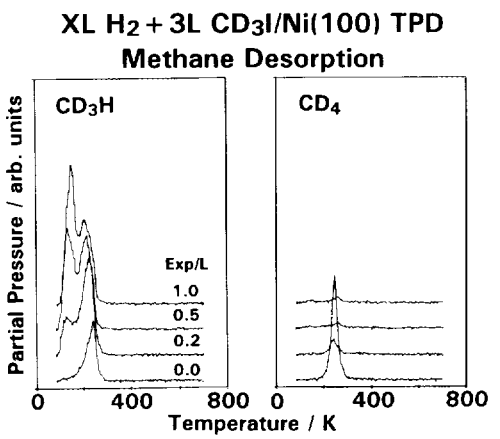


FIG. 10. $CHD_3$ (a, left) and $CD_4$ (b, right) TPD spectra from 3 L $CD_3I$ adsorbed on a Ni(100) surface previously exposed to various doses of hydrogen.

Figure 10 shows methane TPD spectra from hydrogen coadsorbed with 3 L $CD_3I$. In this case both $CHD_3$ and $CD_4$ do form from $CD_3I$ even when adsorbed alone on Ni(100); $CHD_3$ production is explained by incorporation of background hydrogen into the deuterated methyl groups, while $CD_4$ adsorption is due to deuteration with atoms from $CD_3$ surface decomposition. Coadsorbed hydrogen inhibits the decomposition of the methyl groups as in the other systems, so after a 1-L $H_2$ predose no significant $CD_4$ desorption is seen in the TPD (a very small amount of $CD_4$ is always present due to reactions on surface defects). The yield for $CHD_3$ formation increases with hydrogen predose, and the TPD trace splits into two peaks, with the lower temperature one (150 K) dominating at high $H_2$ exposures. The inhibition of the decomposition pathway for $CD_3$ species is also supported by the disappearance of the $D_2$ and HD TPD peaks with $H_2$ coadsorption (Fig. 11).

Finally, the signal intensities from all these TPD experiments were calibrated using a procedure described in a previous publication (*18*); the resulting yields for methane formation are summarized in Fig. 12. The data in Figs. 12a–12c show that for a 1-L methyl iodide dose the presence of coadsorbed hydrogen increases the amount of

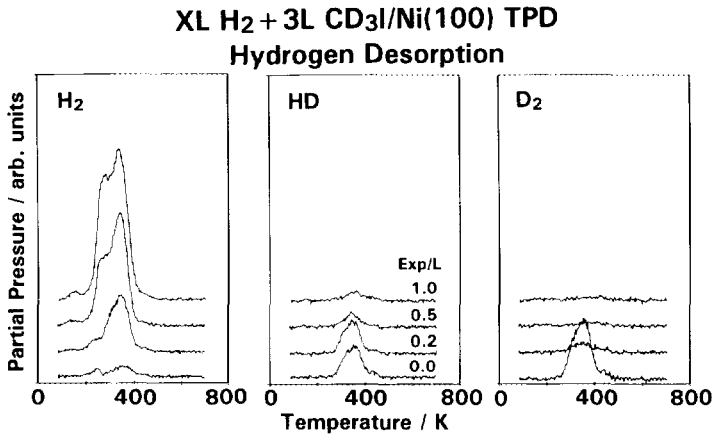


FIG. 11. $H_2$ (a, left), HD (b, center), and $D_2$ (c, right) TPD spectra from 3 L $CD_3I$ adsorbed on a Ni(100) surface previously exposed to various doses of hydrogen.

methane produced by up to a factor of five as the dehydrogenation of the methyl species is inhibited. Furthermore, the increase in methane formation in the case of $H_2$ coadsorption with 1 L $CD_3I$ (Fig. 12c) is all in $CHD_3$, because $CD_4$ production requires the incorporation of deuterium atoms which can only be generated from the decomposition of $CD_3$ species, a process that is inhibited by hydrogen coadsorption as mentioned above. For coverages of methyl iodide near saturation (3 L) the presence of coadsorbed hydrogen also results in an enhancement in methane formation, but the yield in these cases only goes up by about a factor of two (Fig. 12d–12f). In the case of $CH_3I$ coadsorbed with deuterium the $CH_3D$ yield reaches a value of about 0.2 monolayers,

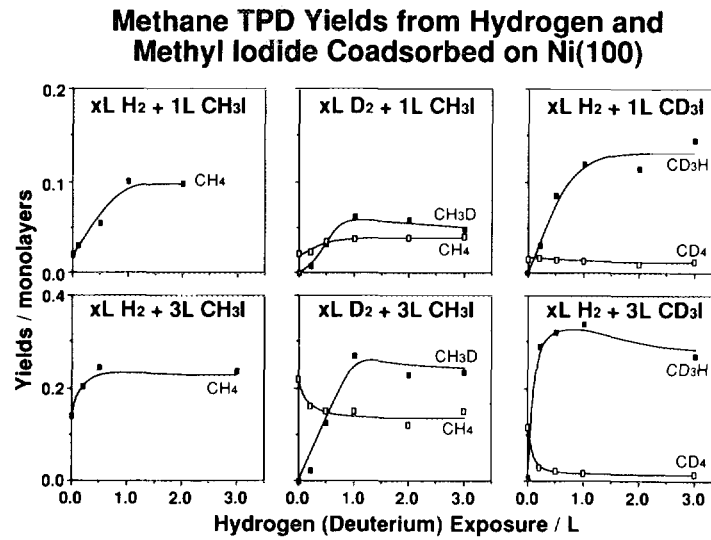


FIG. 12. Methane yields from different TPD experiments with methyl iodide as a function of hydrogen (or deuterium) preexposures: (a) $H_2$ + 1L $CH_3I$, (b) $D_2$ + 1L $CH_3I$, (c) $H_2$ + 1L $CD_3I$, (d) $H_2$ + 3L $CH_3I$, (e) $D_2$ + 3L $CH_3I$, and (f) $H_2$ + 3L $CD_3I$.

and some $CH_4$ is also formed, especially in the low-temperature methane TPD peak. The formation of both types of methane in significant quantities is a reflection of a normal kinetic isotope effect in the competition between incorporation of background hydrogen and predosed deuterium into the methyl group, the reaction with hydrogen being about three to five times faster than with deuterium. The $CH_4$ yield does decrease slightly with increasing coverage, presumably because at least some of the surface hydrogen needed for the production of this molecule initially comes from $CH_3$ decomposition, a pathway that disappears almost entirely when the deuterium is coadsorbed. Finally the yield for $CHD_3$ production from coadsorbed $H_2$ and $CD_3I$ also goes up as expected, and the $CD_4$ yield is reduced to almost zero because of the unavailability of D atoms on the surface for recombination with $CD_3$ species when no decomposition takes place (Fig. 12f).

In order to better understand the mechanism for the low temperature methane formation, which is seen only in the presence of $H_2$ or $D_2$ coadsorption, a series of new experiments were carried out. First, TPD spectra were obtained from surfaces prepared by first dosing 3 L $CD_3I$ either alone or after given exposures of hydrogen at 90 K, and then annealing to various temperatures below 200 K (Fig. 13). Figure 13a shows that in the absence of coadsorbed hydrogen $CHD_3$ and $CD_4$ desorb around 220 and 250 K respectively, and that neither the shape nor the intensity of the $CHD_3$ TPD peak, which originates from the reductive elimination of methyl groups with hydrogen from the background, changes when annealing to temperatures below 200 K before recording the desorption spectra; only after annealing to 200 K the methane peak becomes smaller because some methane desorption starts to take place at that temperature. These results suggest that the annealing process itself does not alter either the nature or the concentration of the species present on the surface in this case. In

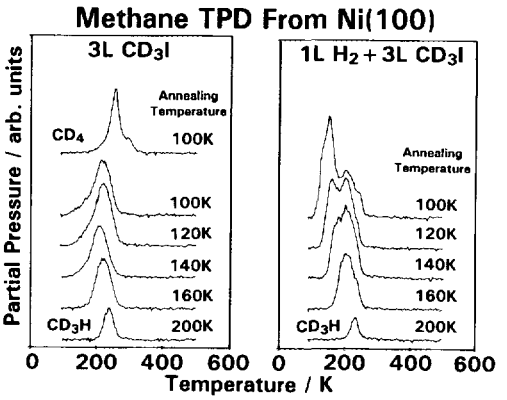


FIG. 13. $CHD_3$ and $CD_4$ TPD spectra obtained after dosing 3 L $CD_3I$ on a Ni(100) surface, clean (a, right) and after a predose of 1 L hydrogen (b, left) at 90 K, and then annealing to the indicated temperatures.

contrast, the TPD traces obtained from the coadsorbed system do change with preannealing of the sample (*19*): two distinct peaks are seen at about 160 and 220 K when adsorption is done at liquid-nitrogen temperatures (the low-temperature peak being about two times larger than the higher temperature one), but a steady decrease of the low-temperature peak takes place with increasing annealing temperature. The high-temperature feature remains unaffected until annealing to 200 K, at which point the yield of that peak is also reduced.

XPS experiments were performed on the same system in order to correlate the rates of the C–I bond scission step with those for methane formation. Fig. 14, which displays iodine $3d_{5/2}$ XPS spectra obtained after dosing the nickel surface with both hydrogen and methyl iodide at 90 K and then annealing it to the indicated temperatures, shows that the I $3d_{5/2}$ XPS binding energy shifts from 620.3 eV at low temperatures (a value that corresponds to molecular methyl iodide) to 619.9 eV above 160 K (a number associated with the atomic iodine that results from C–I bond dissociation). Additional isothermal kinetic determinations, done by following the changes in signal intensity at 620.4 eV as a function of time,

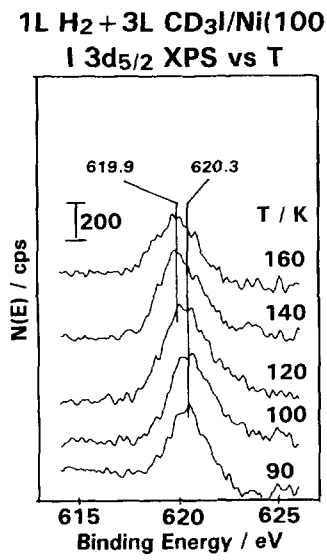


FIG. 14. Iodine $3d_{5/2}$ XPS spectra obtained for a Ni(100) surface dosed sequentially with 1 L $H_2$ and 3 L $CD_3I$ and then annealed to the indicated temperatures.

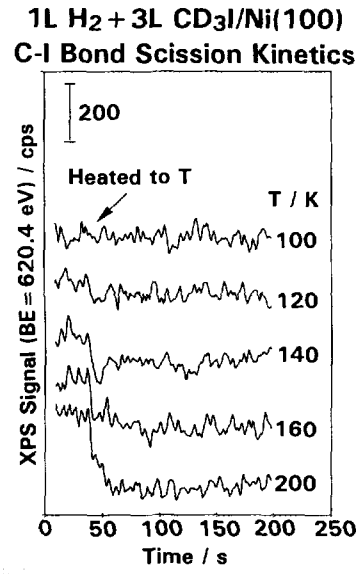


FIG. 15. Time evolution of the XPS signal intensity at 620.4 eV binding energy from 1 L $H_2$ + 3 L $CD_3I$ dosed on Ni(100) while holding the surface temperature to the indicated values.

show that heating to temperatures above 120 K leads to a quick drop in signal intensity until reaching a new value which is still higher than that corresponding to total C–I bond scission (Fig. 15). These results indicate that there are two distinct kinetic regimes for this bond scission step with two clearly different time constants (*19*). The fraction of the iodine XPS signal intensity lost in the initial stage of these annealing experiments (relative to that at 200 K) correlates well with the respective losses in methane TPD peak areas seen in Fig. 13 (*19*).

Finally, the possible formation of methylene during the decomposition of adsorbed methyl iodide was explored by studying the thermal chemistry of $CH_2I_2$ on Ni(100). Figure 16 shows I $3d_{5/2}$ XPS spectra for 6 L $CH_2I_2$ dosed at 90 K and annealed to the indicated temperatures. As with $CH_3I$, the iodine peak shifts, from about 619.9 eV at 90 K to 619.3 eV after heating to 180 K, because the C–I bonds break around those temperatures; that reaction leads to the formation of $CH_2$ species on the nickel surface. TPD spectra from a surface dosed with 10

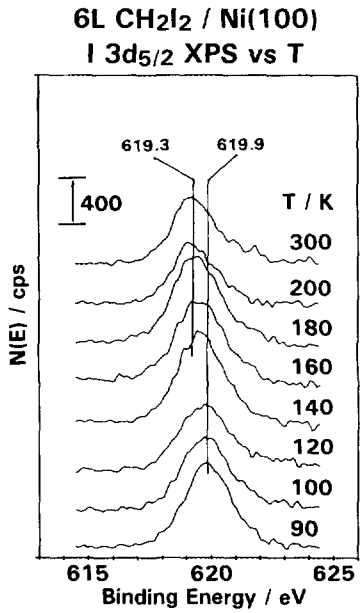


FIG. 16. Iodine $3d_{5/2}$ XPS spectra for 6 L $CH_2I_2$ dosed on Ni(100) after annealing to the indicated temperatures.

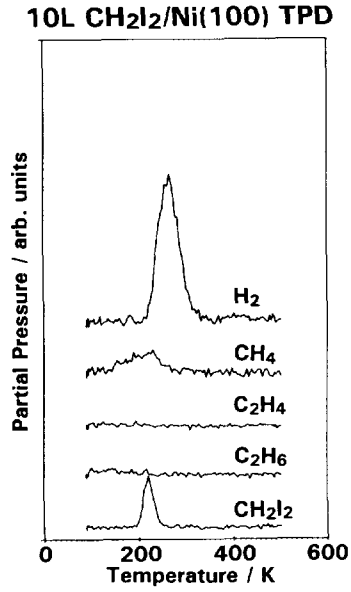


FIG. 17. $H_2$, $CH_4$, $C_2H_4$, $C_2H_6$, and $CH_2I_2$ TPD spectra from 10 L $CH_2I_2$ adsorbed on a Ni(100) surface.

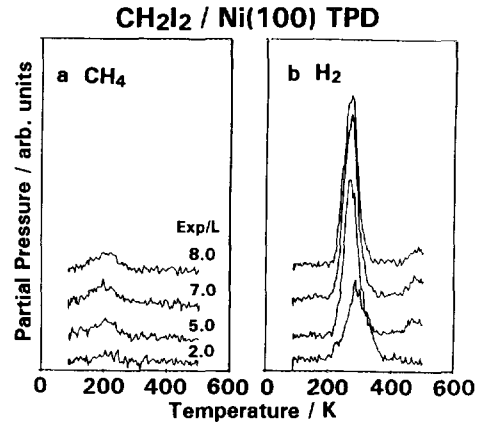


FIG. 18. $CH_4$ (a, left) and $H_2$ (b, right) TPD spectra from $CH_2I_2$ adsorbed on Ni(100) as a function of initial exposure.

L $CH_2I_2$ indicate that most of this methylene dehydrogenates completely to atomic carbon and hydrogen but that some methane is formed as well (Fig. 17); a little molecular desorption is also detected at this coverage, but no dimerization products such as ethane or ethylene were ever seen in these experiments. Additional TPD spectra obtained as a function of initial exposure, shown in Fig. 18, indicate that the hydrogen desorption maxima shift from slightly above 300 K to about 265 K as the coverage is increased, and that its yield almost doubles when going from 2 to 5 L $CH_2I_2$ exposure (saturation is reached around 8 L). Methane formation is only seen as a small and broad peak around 230 K and only after exposures above 5 L, but the yield for this reaction is enhanced by the presence of coadsorbed hydrogen (or deuterium). Figure 19 shows that the yield for $CH_2D_2$ desorption increases significantly when deuterium is preadsorbed on the surface: two broad peaks are seen in the TPD spectra in this case, with the lower temperature methane peak at about 170 K becoming the main feature as the coadsorption $D_2$ increases from 0.2 to 2.0 L. The desorption of methane at 170 K and at 230 K corresponds to processes with apparent activation energies of about 10.5 and 14.5 kcal/mol, respectively. The coadsorption experiments also yield small amounts of $CH_3D$ and

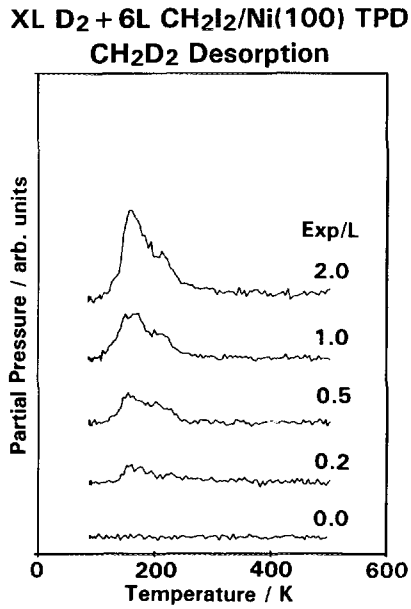


FIG. 19. $CH_2D_2$ TPD spectra from 6 L diiodomethane adsorbed on Ni(100) following various deuterium exposures.

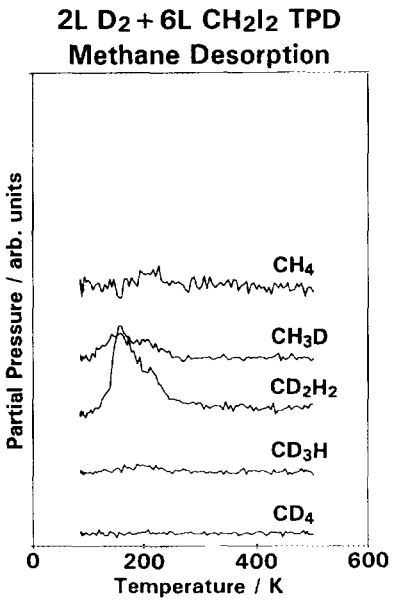


FIG. 20. $CH_4$, $CH_3D$, $CH_2D_2$, $CHD_3$, and $CD_4$ TPD spectra for 2 L $D_2$ and 6 L $CH_2I_2$ coadsorbed on Ni(100).

$CH_4$ (by incorporation of hydrogen from the background), but no $CHD_3$ or $CD_4$ formation is observed in any case, a result that rules out the possible formation of CH groups before the hydrogenation steps take place (Fig. 20).

## 4. DISCUSSION

The results presented in this paper provide data that aid in the determination of the mechanism for the thermal reactions of methyl iodide when adsorbed on Ni(100) surfaces. In our previous studies we had shown that when methyl iodide is adsorbed on a clean Ni(100) the cleavage of the C–I bond occurs readily between 120 and 160 K, as indicated by the shift in binding energy observed in both the I 3*d* and the C 1*s* XPS spectra (*18*). We also determined that this dissociation requires quite a low activation energy, about 3.5 kcal/mol (*17*), and that it leads to the formation of methyl species and iodine atoms on the surface. Depending on the initial methyl iodide coverage the methyl species then either decompose to carbon and hydrogen or undergo hydrogenation to form methane: below 1.5 L $CH_3I$ the dehydrogenation pathway takes place almost exclusively, but at saturation coverages formation of methane occurs below 255 K and becomes dominant (yielding methane to the extent of 70% or more of the total initial methyl iodide). Also, at low methyl iodide coverages hydrogen desorption occurs in a single peak around 370 K, but after higher initial exposures it splits into two peaks centered at about 310 and 375 K; a third small peak was sometimes seen in those spectra at 400 K because of dehydrogenation of either methyl iodide or methyl species on surface defect sites. Finally, molecular desorption of methyl iodide at 145 K was observed only after saturation of the first layer (doses in excess of 3 L).

Coadsorbed hydrogen affects the surface chemistry of methyl iodide in several ways. For one, the presence of such coadsorbed hydrogen reduces the availability of sites for methyl iodide decomposition, and therefore, for the same methyl iodide dose (which yield approximately the same surface coverage), the amount of molecular desorption increases with hydrogen precoverage (Fig. 2c). Hydrogen coadsorption also modifies the rate at which the C–I bond in adsorbed methyl iodide dissociates. Total dissociation in this case occurs below 160 K, the same as in the absence of any coadsorbed hydrogen, but the XPS experiments show that the kinetics of the reaction does not follow the simple exponential decay seen for pure methyl iodide but displays two distinct kinetic regimes instead, an initial sudden fast decomposition of a fraction of the coadsorbed molecules, and a more gradual dissociation of the remaining species. The high temperature slow signal decay resembles that seen for $CH_3I$ adsorbed alone on Ni(100) (*18*), but the low temperature behavior indicates that another C–I bond scission pathway opens up in the presence of surface hydrogen, one that is also related to the formation of methane around 150 K. In cases where both H and D are available on the

surface, $CH_4$ is seen to form preferentially in the low temperature regime (at about 5–10 K lower temperature than $CH_3D$, Figs. 4 and 7), indicating that this reaction displays a normal kinetic isotope effect equivalent to a difference in energy of about 0.5–1.0 kcal/mol. This fact in turn leads to the conclusion that hydrogen atoms must be directly involved in the slow step of this low temperature methane formation; we suggest a mechanism involving the direct attack of a hydrogen atom to the C–I bond of the methyl iodide to form methane and iodine atom (*19*). Formation of methyl free radicals, a mechanism proposed for other systems (*23*), is not likely to occur in this case, since radical recombination pathways are usually accompanied by the formation of coupling hydrocarbon products such as ethane or ethylene; no other hydrocarbon products were detected here besides methane.

As mentioned above, the high temperature C–I bond dissociation kinetics in the coadsorbed case parallels that seen for methyl iodide adsorbed alone on clean Ni(100) surfaces. A combination of TPD, XPS, and SSIMS experiments were used previously to determine that methyl groups form in the latter case below 200 K (*18*); here we make the case for a similar behavior in the former situation. The main piece of evidence for methyl formation when hydrogen is coadsorbed on the surface comes from the TPD results that show that a significant fraction of the adsorbed methyl iodide molecules react to form methane above 200 K. Isotopic labelling experiments proved that such methane is the product of a direct recombination of methyl surface groups with atomic hydrogen: $CHD_3$ was the main desorption molecule detected in experiments where $H_2$ was coadsorbed with $CD_3I$ and, likewise, TPD of $D_2$ adsorbed with $CH_3I$ generated mostly $CH_3D$. No evidence for the formation of either $CH_2$ (methylene) or CH (methylidyne) was seen in any of our experiments: TPD from $D_2$ coadsorbed with $CH_3I$ does not yield any $CH_2D_2$ or $CHD_3$ (Fig. 3), and no $CH_2D_2$ is detected in $H_2$ + $CD_3I$ TPD experiments either. The lack of methane desorption with such isotopic composition not only proves that methyl moieties formed from methyl iodide dissociation are the only species responsible for the methane production, but also rules out any H–D exchange reactions on the surface under these conditions. Methylene formation can also be discarded based on the results from studies on the chemistry of methylene species prepared by thermal decomposition of $CH_2I_2$, which showed that the hydrogenation of those moieties is facile in the presence of coadsorbed deuterium; $CH_2D_2$ desorbs in these experiments at temperatures as low as 160 K (Fig. 19). The lack of $CH_2$ formation from methyl decomposition sets a lower limit for the activation energy of the initial dehydrogenation reaction above 10 kcal/mol, and the lack of $CHD_3$ desorption from coadsorption experiments with deuterium and diiodomethane indicate that a similarly high energy barrier exists for the dehydrogenation of methylene to methylidyne. These observations are consistent with results reported by Zhou and White (*24*), who found that at low coverages methyl groups decompose to C and H on the surface without any accumulation of $CH_2$ and CH. In addition, methane formation from $CH_2I_2$ adsorbed alone at 230 K requires about the same activation energy as that for saturation coverages of methyl species, and is most probably limited by the supply of hydrogen atoms on the surface (which originate from the dehydrogenation of $CH_2$ groups), while desorption at 170 K in the presence of surface deuterium must be limited by the recombinatory hydrogenation steps. Since methane formation in the latter case occurs at temperatures comparable with those seen for methyl groups, we conclude that the last hydrogenation step is rate limiting, and that therefore methyl species are more stable than methylene moieties; methylene can be converted to methyl and eventually to methane, but methyl conversion to methylene is a more difficult reaction.

Preadsorbed hydrogen inhibits the decomposition of adsorbed methyl species as well: the data in Figs. 5a and 6a show that the amount of $H_2$ desorption from $CH_3I$ decomposition decreases to almost zero as $D_2$ is preadsorbed on the surface, and Figs. 9c and 11c show that the amount of $D_2$ generated from the decomposition of $CD_3I$ also disappears as large amounts of $H_2$ are coadsorbed. It is clear that there is a significant change in selectivity from decomposition to reductive elimination and methane formation as the surface is precovered with hydrogen: for 1 L $CH_3I$ the yield for methane formation ($CH_4$) increases by about five times when hydrogen is predosed on the surface (Fig. 12a), and in the case of $D_2$ coadsorption with 1 L $CH_3I$ both $CH_4$ and $CH_3D$ desorption yields also increase significantly. The inhibition of the dehydrogenation steps can be seen in the results from methane TPD experiments as well: for instance, in $H_2$ coadsorption experiments with $CD_3I$ a large increase in $CHD_3$ production is detected, very little of $CD_4$ is formed (Figs. 12c and f), and no deuterium desorption is observed at all (Figs. 9 and 11).

Finally, a significant change in the energetics of the desorption of the predosed hydrogen was also observed in the coadsorbed systems: one peak due to the normal recombination of hydrogen atoms is always seen around 350 K, but, in addition, a second peak develops around 260 K at saturation (Figs. 1b, 2b, 5c, 6c, 9a, and 11a). This latter feature is probably the result of a repulsive interaction between the adsorbed hydrogen and the surface iodine atoms deposited by the C–I bond scission step; it is clear that it does not originate directly from methyl iodide decomposition, because when $D_2$ is coadsorbed with $CH_3I$, the low-temperature peak is mainly composed of $D_2$ (Fig. 6), and in the case of $H_2$ and $CD_3I$ this feature is only seen in the $H_2$ TPD trace (Fig. 11).

The results reported here can be related to the behavior of nickel catalysts in hydrocarbon conversion processes such as H–D exchange, which is the simplest reaction that measures kinetic activities for hydrogenation/dehydrogenation reactions on alkyl groups. In his original work Kemball reported that nickel films are good catalysts for inducing multiple exchange of methane with deuterium, the main products observed being $CH_3D$ and $CD_4$ (*25*). Subsequent studies, however, have shown that the relative selectivity between the single and multiple exchange mechanisms depends strongly on both the temperature and the partial pressures used for the reaction: it has been generally observed that $CH_3D$ formation is favored either by low temperatures or by high deuterium partial pressures (*26–28*). This fact is manifested in the values reported for the activation energies and the deuterium reaction orders for both pathways, which range from 10 to 24 kcal/mol and from $-0.78$ to 0.15 for the single exchange, and from 18 to 43 kcal/mol and from $-1.02$ to $-0.38$ for the multiple exchange, respectively (*26–29*). The ranges displayed by those numbers are quite broad, specially since they represent a summary from several different reports, but what is clear in all the studies published to date is that the multiple exchange always displays higher activation energies and a more negative order dependence on deuterium partial pressure than the single deuterium replacement. This fact could explain why we do not observe any exchange in our experiments. For one, they were done under untrahigh vacuum conditions, and they emulate high deuterium partial pressure conditions since deuterium is adsorbed on the surface prior to methyl iodide dosing (*27*). In addition, the nature of thermal-programmed desorption experiments, where the sample temperature is ramped as the desorption products are detected, favors the pathways that display the lowest activation energies. From the data obtained here we estimate the barrier for $CD_4$ production from normal methyl groups and deuterium, a reaction that requires going through the formation of methylene moieties, to be larger by a few kcal/mol than that for $CH_3D$ formation. We should point out that in the case of platinum

the opposite is true, substantial multiple exchange was observed in that system even in TPD experiments under vacuum conditions (*11, 30, 31*).

Nickel catalysts are also well known methanation catalysts (*32*). Many studies have shown that the catalytic conversion of $CO/H_2$ mixtures yield methane almost exclusively without the formation of any significant quantities of heavier hydrocarbons. The most accepted mechanism proposed for this reaction is one that involves the initial dissociation of CO molecules to yield atomic C and O atoms on the surface and the subsequent hydrogenation of the surface carbide to methane by coadsorbed hydrogen (*33–36*). The activation energy for this latter reaction has been reported to be bewteen 17 and 30 kcal/mol on supported catalysts depending on the reaction conditions (*37–39*), and about 22–25 kcal/mol on nickel single crystal surfaces (*40–42*). In our studies we have demonstrated that both $CH_2$ and $CH_3$ species hydrogenate quite easily to produce methane (they display an activation barrier of 10 kcal/mol or less), and that methyl species are more stable than methylene moieties on the Ni(100) surface since methylene hydrogenates to methyl at a faster rate than that with which methyl hydrogenates to methane. These results lead to the conclusion that the limiting step in the hydrogenation of carbidic carbon on the surface must be one of the initial hydrogen incorporation steps, those that form either the methylidyne (CH) or the methylene ($CH_2$) surface intermediates. What is clear from both ours and previously reported results is that the principal reactions that $CH_x$ fragments follow on nickel metal surfaces in the presence of coadsorbed hydrogen are hydrogenation–dehydrogenation steps and not dimerization or polymerization reactions. It is interesting to notice that such carbon–carbon bond forming reactions have been seen on both copper and silver surfaces (*43–44*); those metals are noticeably poor catalysts for the incorporation or the removal of hydrogen atoms from hydrocarbon surface species.

Summarizing the discussion presented above, when hydrogen is coadsorbed with methyl iodide on Ni(100) surfaces methane forms in two temperature regimes and by following two different mechanisms. Our kinetic experiments indicate that the formation of methane at low temperatures (around 150 K) is limited by the rate of the C–I bond breaking step, and that it requires the direct paticipation of surface hydrogen atoms; the mechanism for this reaction may therefore involve a direct attack of a hydrogen atom to a methyl iodide molecule, with the formation of methane and the dissociation of C–I bond taking place simultaneously in a concerted fashion. The high-temperature methane formation (about 250 K), on the other hand, is believed to involve the reductive elimination of the surface methyl groups that form after C–I bond scission in adsorbed methyl iodide molecules. A careful analysis of the desorption traces for this case indicates that the kinetic behavior of this reaction is not simple, but even though the energy barrier for the reductive elimination step is probably on the order of 10 kcal/mol or less (*18*), it is much larger than the 3–4 kcal/mol required for the activation of the C–I bond (*17*): clearly, methane desorption (in the high-temperature regime) always occurs after the formation of methyl surface groups reaction is complete. It was also determined here that methyl species do not decompose to $CH_2$ in the presence of coadsorbed hydrogen, and furthermore, that the formation of methane from hydrogenation of methylene groups is quite facile, taking place around 230 K when adsorbed alone, and at about 170 K in the presence of coadsorbed deuterium.

ACKNOWLEDGMENTS

Financial support for this research was provided by a grant from the National Science Foundation (CHE-9222164).

REFERENCES

1. Zaera, F., *Acc. Chem. Res.* **25,** 260 (1992).
2. Somorjai, G. A., *Catal. Rev.-Sci. Eng.* **23,** 189 (1981).

3. Biloen, P., and Sachtler, W. M. H., *Adv. Catal.* **30,** 165 (1981).
4. Bell, A. T., *Catal. Rev.-Sci. Eng.* **23,** 203 (1981).
5. Davis, S. M., and Somorjai, G. A., *in* "The Chemical Physics of Solid Surfaces and Heterogeneous Catalysis" (D. A. King and D. P. Woodruff, Eds.), Vol. 4, p. 217. Elsevier, Amsterdam, 1982.
6. Ogle, K. M., and White, J. M., *Surf. Sci.* **165,** 234 (1986).
7. Zaera, F., and Somorjai, G. A., *in* "Hydrogen Effects in Catalysis: Fundamentals and Practical Applications" (Z. Paál and P. G. Menon, Eds.), p. 425. Dekker, New York, 1988.
8. Zaera, F., *J. Catal.* **121,** 318 (1990).
9. Zaera, F., *J. Phys. Chem.* **94,** 5090 (1990).
10. Zhou, X.-L., and White, J. M., *Surf. Sci.* **194,** 438 (1988).
11. Zaera, F., *Surf. Sci.* **262,** 335 (1992).
12. Zaera, F., *Surf. Sci.* **219,** 453 (1989).
13. Zaera, F., *J. Am. Chem. Soc.* **111,** 8744 (1989).
14. Zaera, F., *J. Phys. Chem.* **94,** 8350 (1990).
15. Zaera, F., and Hoffmann, H., *J. Phys. Chem.* **95,** 6297 (1991).
16. Hoffmann, H., Griffiths, P. R., and Zaera, F., *Surf. Sci.* **262,** 141 (1992).
17. Tjandra, S., and Zaera, F., *J. Vac. Sci. Technol. A* **10,** 404 (1992).
18. Tjandra, S., and Zaera, F., *Langmuir* **8,** 2090 (1992).
19. Tjandra, S., and Zaera, F., *J. Am. Chem. Soc.* **114,** 10645 (1992).
20. Jenks, C. J., Bent, B. E., Bernstein, N., and Zaera, F., *J. Am. Chem. Soc.* **115,** 308 (1993).
21. Redhead, P. A., *Vacuum* **12,** 203 (1962).
22. Habenschaden, E., and Kupper, J., *Surf. Sci.* **138,** L147 (1984).
23. Jenks, C. J., Chiang, C.-M., and Bent, B. E., *J. Am. Chem. Soc.* **113,** 6308 (1991).
24. Zhou, X.-L., and White, J. M., *Chem. Phys. Lett.* **142,** 376 (1987).
25. Kemball, C., *Proc. R. Soc. London Ser. A* **207,** 539 (1951).
26. Cece, J. M., and Gonzalez, R. D., *J. Catal.* **28,** 260 (1973).
27. Leach, H. F., Mirodatos, C., and Whan, D. A., *J. Catal.* **63,** 138 (1980).
28. Dalmon, J. A., and Mirodatos, C., *J. Mol. Catal.* **25,** 161 (1984).
29. Kemball, C., *Proc. R. Soc. A* **217,** 376 (1953).
30. Zaera, F., *Langmuir* **7,** 1998 (1991).
31. Zaera, F., *Catal. Lett.* **11,** 95 (1991).
32. Vannice, M. A., *Catal. Rev.-Sci. Eng.* **14,** 153 (1976).
33. Araki, M., and Ponec, V., *J. Catal.* **44,** 439 (1976).
34. Biloen, P., Nelle, J. N., and Sachtler, W. M. H., *J. Catal.* **58,** 95 (1979).
35. Goodman, D. W., and Yates, J. T., Jr., *J. Catal.* **82,** 225 (1983).
36. Kaminsky, M. P., Winograd, N., and Geoffroy, G. L., *J. Am. Chem. Soc.* **108,** 1315 (1986).
37. Bousquet, J. L., and Teichner, S. J., *Bull. Soc. Chim. Fr.*, 2963 (1969).
38. Dalla Beta, R. A., Piken, A. G., and Shelef, M., *J. Catal.* **40,** 173 (1975).
39. Vannice, M. A., *J. Catal.* **44,** 152 (1976).
40. Goodman, D. W., Kelley, R. D., Madey, T. E., and Yates, J. T., Jr., *J. Catal.* **63,** 226 (1980).
41. Goodman, D. W., Kelley, R. D., Madey, T. E., and White, J. M., *J. Catal.* **64,** 479 (1980).
42. Goodman, D. W., *Acc. Chem. Res.* **17,** 194 (1984).
43. Chiang, C.-M., Wentzlaff, T. H., Jenks, C. J., and Bent, B. E., *J. Vac. Sci. Technol. A* **10,** 2185 (1992).
44. Zhou, X.-L, and White, J. M., *J. Phys. Chem.* **95,** 5575 (1991).